



Full Text View

[Volume 31, Issue 10 \(October 2001\)](#)

Journal of Physical Oceanography

 Article: pp. 2944–2957 | [Abstract](#) | [PDF \(1.30M\)](#)

Evidence for Coupled Rossby Waves in the Annual Cycle of the Indo–Pacific Ocean

Warren B. White
Scripps Institution of Oceanography, University of California, San Diego, La Jolla, California

(Manuscript received February 1, 2000, in final form February 28, 2001)

DOI: 10.1175/1520-0485(2001)031<2944:EFCRWI>2.0.CO;2

ABSTRACT

The annual cycle in TOPEX/Poseidon sea level height (SLH) and National Centers for Environmental Prediction (NCEP) sea surface temperature (SST) and meridional surface wind (MSW) from 1993 to 1998 in the trade wind zone over the Indo-Pacific Ocean from 5° to 25° latitude in both hemispheres is examined. Zonal wavenumber–frequency spectra of monthly mean SLH, SST, and MSW residuals about the annual mean find peak spectral energy density for westward-propagating waves of annual period and basinscale wavelengths in all three variables. Moreover, spectral coherence and phase between the three variables are significant, with warm SST residuals displaced 0°–90° of phase to the west of high SLH residuals, and poleward MSW residuals displaced 0°–90° of phase to the east of warm SST residuals, similar to those observed for coupled Rossby waves on interannual period scales. Removing zonal means at each latitude from the annual cycle in SLH, SST, and MSW allows westward phase propagation to be observed in each variable, together with poleward refraction stemming from the reduction in westward phase speed with latitude. The fact that the latter occurs in both oceanic and atmospheric variables indicates that annual Rossby waves in the ocean are coupled to the overlying atmosphere. The reduction in westward phase speed with latitude (and, hence, the poleward refraction) is less than expected for free Rossby waves, with the apparent coupled Rossby waves traveling faster (slower) poleward (equatorward) of ~ 12° latitude.

Table of Contents:

- [Introduction](#)
- [Data and methods](#)
- [Zonal wavenumber–frequency](#)
- [Time–longitude](#)
- [Westward phase speeds](#)
- [Phase relationships between](#)
- [Poleward refraction patterns](#)
- [Discussion and conclusions](#)
- [REFERENCES](#)
- [FIGURES](#)

Options:

- [Create Reference](#)
- [Email this Article](#)
- [Add to MyArchive](#)
- [Search AMS Glossary](#)

Search CrossRef for:

- [Articles Citing This Article](#)

Search Google Scholar for:

- [Warren B. White](#)

1. Introduction

[White \(1977\)](#) observed what appeared to be baroclinic Rossby wave activity in the annual cycle of upper-ocean thermocline temperatures southeast of Hawaii in a grid of bathythermograph observations extending from 10° to 19°N and

157° to 148°W, repeated each month for 17 months from February 1964 to June 1965 (Charnel et al. 1967). These annual Rossby waves propagated westward and poleward through the grid with zonal speeds of 0.40 m s^{-1} near 11°N , and decreasing to 0.15 m s^{-1} near 18°N . This decrease in westward phase speed with latitude was consistent with baroclinic Rossby wave theory (e.g., Veronis and Stommel 1956), yielding a poleward refraction of the waves consistent with the theoretical generation at the west coast of North America one year earlier. Shortly thereafter, Meyers (1979) examined annual Rossby waves in thermocline temperatures between 6° and 18°N in the tropical North Pacific Ocean, finding them propagating westward from 0.50 to 0.60 m s^{-1} near 6°N , and decreasing poleward from 0.10 to 0.20 m s^{-1} near 18°N , the latter speeds similar to those observed by White (1977) southeast of Hawaii. Subsequently, Kang and Magaard (1980) examined annual Rossby waves in thermocline temperatures from 32° to 40°N in the North Pacific Ocean, finding them traveling westward and poleward at 0.01 to 0.02 m s^{-1} , an order of magnitude smaller than the speeds observed southeast of Hawaii by White (1977) but consistent with Rossby wave theory. In the present study, we find evidence for the tropical annual Rossby waves of White (1977) and Meyers (1979) to be coupled to the overlying atmosphere.

At the time White (1977) proposed that annual Rossby waves could be generated by the annual cycle in surface wind stress curl (WSC), which on basinscales was expected to yield wind-forced Rossby waves with a perceived westward phase speed twice that of free Rossby waves. At the same time, Magaard (1977) proposed the entire spectrum of Rossby waves on intra-annual, annual, and interannual frequencies to be forced by WSC and buoyancy flux anomalies. This latter work presumed atmospheric forcing to be characterized by white noise, with Rossby waves responding in damped resonance, yielding peak spectral energy density along the Rossby wave dispersion curve in zonal wavenumber–frequency spectra. Subsequently, Kang and Magaard (1979) and Kang et al. (1982) proposed that Rossby wave activity could be either wind forced or arise from instabilities in the background shear flow. White (1977), Meyers (1979), and White and Saur (1981) proposed that free annual Rossby waves could be generated at the eastern boundary, but anomalous WSC forcing would modify them as they propagated westward across the ocean. The latter view was supported by theoretical and modeling studies by Mysak (1983) and Cummins et al. (1986). By 1985 or so, observations and theory firmly established Rossby wave activity across a broad spectrum to be either wind or stability forced, not composed of free waves; as such their speeds could be faster or slower than those expected of free waves, with wind forcing making them go faster and instability mechanisms making them go slower.

Since their initial discovery, many studies have observed wind-forced annual and interannual Rossby waves (e.g., Meyers 1979; White and Saur 1981, 1983; Price and Magaard 1983; White 1983, 1985; White et al. 1985a,b, 1989; Pazan and White 1987; Graham and White 1988; Kessler 1990; Perigaud and Delecluse 1993; Masumoto and Meyers 1998). Recently Qiu et al. (1997) invoked wind forced Rossby waves to explain faster than expected westward phase speeds observed in extratropical thermocline temperatures (White et al. 1985a; Kessler 1990) and in extratropical sea level heights (Chelton and Schlax 1996). As an alternative explanation for these faster Rossby wave speeds in the extratropics, Killworth et al. (1997) constructed a continuously stratified model for baroclinic Rossby waves wherein the shear flow in the main pycnocline yields free waves that propagate faster to the west than is possible with two-layer models (e.g., Veronis and Stommel 1956). Shortly thereafter, Dewar (1998) constructed a three-layer model for baroclinic Rossby waves, yielding faster waves in the midlatitude portion of the subtropical gyre and slower waves in the subtropical portion. At about this same time, Cipollini et al. (1997) observed Rossby wave activity at 34°N in the North Atlantic Ocean in both sea level height (SLH) and sea surface temperature (SST) anomalies, finding westward phase speeds consistent with the models of Killworth et al. (1997) and Dewar (1998). On the other hand, Hill et al. (2000) observed Rossby wave activity over the global extratropical ocean utilizing the Along-Track Scanning Radiometer (ATSR), finding westward phase speeds faster than expected from the continuously stratified and multilayered models by 20%–30%. The model by Dewar (1998) offered an explanation of how the westward phase speeds of observed Rossby waves can be less than expected of the free waves in the tropical portions of the subtropical gyres, as observed by White et al. (1985a), Kessler (1990), Chelton and Schlax (1996), White et al. (1998), White (2000b), and Hill et al. (2000).

A number of these earlier studies found interannual Rossby waves in damped resonance with that portion of the anomalous WSC spectrum traveling to the west at Rossby wave speeds (White 1985; White et al. 1985b) as proposed by Magaard (1977). Kessler (1990) also found this to be the case, but he proposed that interannual Rossby waves are not simply forced by white noise WSC forcing in the overlying atmosphere, they are coupled to it. This bold proposition represented a paradigm shift in thinking about the source of oceanic Rossby wave activity, suggesting that anomalous WSC forcing is not of the white noise variety presumed by Magaard (1977) in an uncoupled scenario, but is of the red noise variety expected of covarying SLH and SST anomalies in a coupled scenario. Kessler's (1990) work implied that WSC anomalies, forced by the underlying Rossby waves, would adopt the spectral shape of the oceanic Rossby waves with which they are coupled. In the present study, we find this to be true of meridional surface wind (MSW) anomalies.

White et al. (1998) and White (2000a,b) examined TOPEX/Poseidon SLH anomalies together with National Centers for Environmental Prediction (NCEP) and the National Center for Atmospheric Research (NCAR) SST, sea level pressure (SLP), and MSW anomalies, finding interannual Rossby waves in SLH anomalies in both the tropical and extratropical Indian and Pacific Oceans coupled to the overlying atmosphere. They found interannual coupled Rossby wave activity arising in two different ways. White (2000b) found coupled Rossby waves arising from unstable growth in the interior ocean–

atmosphere system, while [White \(2000a\)](#) found oceanic Rossby waves generated at the eastern boundary and coupled to the overlying atmosphere as they propagate westward away from the boundary. In each of these studies, SLP or MSW anomalies were found to propagate in fixed phase with Rossby wave signatures in covarying SLH and SST anomalies.

The phase relationship between SLH and SST anomalies associated with coupled Rossby waves appears to describe two different thermodynamical relationships. The 90° phase separation observed by [White \(2000b\)](#) in the tropical Pacific Ocean is consistent with SST anomalies deriving from meridional heat advection by geostrophic flow anomalies associated with the Rossby waves in SLH anomalies. On the other hand, the 0° phase separation observed by [White \(2000a\)](#) in the Indian Ocean is consistent with SST anomalies deriving from vertical transfer of heat by entrainment at the base of the near surface mixed layer associated with the Rossby waves in SLH anomalies. In both cases, positive feedbacks from SST-induced changes in SLP and MSW anomalies act through WSC anomalies to alter the westward phase speed of the oceanic Rossby wave in SLH anomalies (that is, retarding or advancing it by generating vortex stretching eastward or westward of wave crests, respectively). This feedback either retards or advances the westward propagation of the Rossby waves depending on the thermodynamics of coupling and the background gradients in the mean upper-ocean temperature field. Coupling also allows growth or decay of the coupled wave amplitude, with stable coupled waves following specific paths (e.g., along SST isotherms) in order to maintain wave amplitude against dissipation.

[White \(2000a,b\)](#) found the case for coupled Rossby waves to be compelling by finding zonal wavenumber–frequency spectra of interannual SLP and MSW anomalies emulating Rossby wave spectra observed in interannual SLH and SST anomalies. Moreover, he found that all three SLH, SST, and SLP variables displayed significant spectral coherence, with oceanic and atmospheric variability propagating westward in fixed phase with one another. This was very different from the situation proposed by [Magaard \(1977\)](#) where Rossby wave spectra were believed to be stochastically forced by white noise WSC spectra. Even so, [Magaard's \(1977\)](#) paradigm may hold for regions where or during periods when coupling is weak or absent, as well as for shorter-scale Rossby wave activity (that is, the mesoscale eddy field). The latter is expected since the ocean and atmosphere can be expected to decouple for some “short” time- and space scales, the threshold of which has yet to be established. Furthermore, [Magaard's \(1977\)](#) paradigm may even hold in the presence of robust coupled Rossby wave activity if uncoupled and coupled waves are sufficiently separated from one another in zonal wavenumber–frequency space. In the latter case, coupled Rossby wave activity can be expected to broaden the band of wavenumbers and frequencies occupied by damped resonant Rossby waves.

Today, more than 20 years after the initial observations of annual Rossby waves in the tropical North Pacific Ocean ([White 1977](#); [Meyers 1979](#); [Kang and Magaard 1980](#)), we are now in position to reexamine these issues utilizing TOPEX/Poseidon SLH data on a global grid ([Fu et al. 1994](#)). This is possible because fluctuations in the depth of the main pycnocline, along which baroclinic Rossby waves propagate as internal waves, are reflected in SLH fluctuations ([Tai et al. 1989](#); [White and Tai 1995](#)). In the present study we examine the TOPEX/Poseidon SLH dataset together with the NCEP–NCAR SST, and MSW datasets for evidence supporting the hypothesis that baroclinic Rossby waves in the annual cycle over the tropical Indo–Pacific Oceans ([Fig. 1a](#)) are coupled to the overlying atmosphere, as observed on interannual period scales ([White et al. 1998](#); [White 2000a,b](#)). In the present analysis, we look for SLH, SST, and MSW residuals to display common peaks in wavenumber–frequency spectra, and to display significant squared coherence and phase. We also look for the three variables to be phase locked with one another as they propagate westward across the ocean, displaying the same characteristic spatial refraction pattern. We also look for whether the meridional profiles of westward phase speeds in each ocean differ significantly from those of free uncoupled Rossby waves, as expected of the coupled Rossby waves ([White et al. 1998](#); [White 2000a,b](#)).

2. Data and methods


We utilize monthly SLH data gridded uniformly over the global ocean for 6 years from January 1993 to December 1998. These SLH data derive from the TOPEX/Poseidon satellite altimeter, remotely sensed along discrete ground tracks laid down by the satellite over the global ocean, with tracks repeated every 10 days. Subsequently, these track SLH data are interpolated onto a 1° latitude–longitude grid each month from 60°S to 60°N by S. Hayashi, V. Zlotnicki, and L. Fu (1998, personal communication). We also utilize SST and MSW data from the NCEP–NCAR reanalysis ([Kalnay et al. 1996](#)). These NCEP–NCAR data are available on a 2° latitude by 2° longitude grid over the global ocean each month.


Prior to analysis we interpolate SLH, SST, and MSW datasets on to a standard 2° latitude by 2° longitude grid, centered at the middle of each month. This yields a 72-month time sequence over the 6 years from 1993–98 at each grid point over the global ocean. Next we compute long-term monthly means at each grid point over the 6 years and subtract these from the long-term annual mean to produce the mean annual cycle, that is, 12 long-term monthly mean differences about the annual mean at each grid point. We also compute monthly residuals about the long-term annual mean over the 6-yr record for the purpose of computing zonal wavenumber–frequency spectra.




In the present study we examine the annual cycle of SLH, SST, and MSW from 5° to 25° in the trade wind zone across the Indo–Pacific Ocean over the 6 years from 1993 to 1998. The idea that baroclinic Rossby wave activity can be detected in satellite SLH datasets ([White et al. 1990a,b](#); [White and Tai 1992](#); [Chelton and Schlax 1997](#); [Cipollini et al. 1997](#)) and in


satellite SST datasets ([Halliwell et al. 1991a,b](#); [Cipollini et al. 1997](#); [Hill et al. 2000](#)) is well established. Now the pertinent issue is whether we can detect baroclinic Rossby wave signatures in overlying atmospheric variables (i.e., SLP, MSW, and/or WSC) as [White et al. \(1998\)](#) and [White \(2000a,b\)](#) were able to do.

3. Zonal wavenumber–frequency spectra of SLH, SST, and MSW differences


We begin by computing zonal wavenumber–frequency spectra of individual monthly SLH, SST, and MSW residuals about the long-term annual mean ([Jackson 1996](#), 295–301) along constant latitudes given by zonal solid lines displayed in the trade wind zone of the Indo-Pacific Ocean ([Fig. 1a](#) ). These spectra are not shown since they yield peak spectral energy density at the annual frequency in each spectrum as expected. Even so, we find peak annual spectral energy densities in the left-hand quadrant exceeding those in the right-hand quadrant at all latitudes. This indicates the dominance of westward phase propagation over eastward phase propagation in the annual cycle for all three variables.



In order to focus on the annual cycle, we bandpass time records of SLH, SST, and MSW residuals for periods ranging from 6 to 18 months and compute the zonal wavenumber–frequency spectra. Furthermore, in order to focus on propagation we subtract the spectral energy density estimates in the right-hand quadrant for positive zonal wavenumbers from those in the left-hand quadrant for negative zonal wavenumbers, yielding positive (negative) spectral energy density of westward-(eastward) propagating waves. These “propagation” zonal wavenumber–frequency spectra eliminate standing wave activity, focusing on the energy density of the dominant propagating wave. These propagation spectra for the Indian, South Pacific, and North Pacific Oceans ([Fig. 2](#) ) indicate westward phase propagation dominating eastward phase propagation in all three variables. We superimpose the free Rossby wave dispersion curve for each latitude on each spectra, the latter yielding constant westward phase speeds in the long-wave limit computed by [Killworth et al. \(1997\)](#).


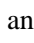
For zonal propagation spectra in [Fig. 2](#)  to share peak spectral energy density near the Rossby wave dispersion curve indicates that annual residuals in both ocean and atmosphere propagate westward together at or near the free Rossby wave phase speeds for the ocean. This is a necessary but not sufficient condition for the presence of coupled Rossby wave activity to exist in the annual cycle. Notice that covariability between ocean and atmosphere in the tropical Pacific Ocean is restricted to the eastern and central oceans ([Fig. 1a](#) ) coinciding with latitude domains of the high annual mean zonal surface winds (ZSW) in the trade wind zone ([Fig. 1b](#) ). This indicates that coupling between ocean and atmosphere requires high background wind speeds. There is a good reason for this. The ocean can only influence the overlying atmosphere through the gradient portion of sensible-plus-latent heat flux residuals (i.e., the portion arising from to air–sea temperature and specific humidity differences), the coefficients of which depend upon the background wind speed ([White et al. 1998](#)). Thus, coupling between ocean and atmosphere, requiring SST residuals to influence MSW residuals in the lower troposphere, can be seen here to be successful in this endeavor in regions of high annual mean ZSW in the trade wind zone of both the Indian and Pacific Oceans.


These propagation spectra for annual SLH, SST, and MSW differences in [Fig. 2](#)  display significant peak spectral energy density for all three variables at similar zonal wavelengths, with the center of shared spectral energy density estimated by the solid circle. In the Pacific (Indian) Ocean, peak spectral energy density at 10° latitude (14°S) overlies the Rossby wave dispersion curve but poleward (equatorward) of this latitude it occurs for lower (higher) zonal wavenumbers. This indicates that covarying SLH, SST, and MSW residuals propagate westward faster (slower) than free Rossby waves poleward (equatorward) of ~10° latitude (14°S) in the tropical Pacific (Indian) Ocean. This is similar to that observed by [White et al. \(1985\)](#), [Kessler \(1990\)](#), [Chelton and Schlax \(1996\)](#), and [Hill et al. \(2000\)](#) in thermocline temperature, thermocline depth, sea level height, and surface temperature anomalies, respectively. Moreover, this is in qualitative agreement with the theoretical development of coupled Rossby waves in the Pacific Ocean ([White et al. 1998](#); [White 2000b](#)), whose westward phase speeds are slower (faster) than free westward phase speeds in the Tropics (extratropics).

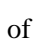
4. Time–longitude diagrams of covarying SLH, SST, and MSW differences

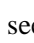
The detection of annual Rossby waves southeast of Hawaii ([White 1977](#)) yielded two hypotheses concerning their source (s): that annual Rossby waves derive from annual fluctuations in the depth of the pycnocline along the west coast of North America and/or from its pumping by WSC anomalies in the eastern tropical North Pacific Ocean. The latter hypothesis was supported by subsequent analysis conducted for annual Rossby waves in the tropical North Pacific Ocean by [Meyers \(1979\)](#). Now we examine time–longitude diagrams of long-term monthly mean SLH, SST, and MSW differences about the long-term annual mean ([Fig. 3](#) ), displaying two cycles of annual variability.


Following the methodology of [White \(1977\)](#), we remove the zonal mean and trend across the trade wind zone (i.e., across the shaded regions in [Fig. 1a](#) ) to enhance westward phase propagation in each variable. Time–longitude diagrams are computed along the zonal solid lines ([Fig. 1a](#) ). In each time–longitude diagram we plot a sloping black line along maximum positive SLH differences; these lines extend from the eastern edge of the diagram as far west as possible while still coinciding with maximum SLH differences. These sloping black lines are repeated in time–longitude diagrams for SST and MSW differences, allowing us to assess the degree of alignment in the westward phase propagation among all three variables. Where black lines violate westward phase propagation in SST and MSW differences, we replace them with

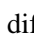
sloping dashed lines). Thus, sloping black lines (sloping dashed lines) in SST and MSW differences show where annual variability in the atmosphere is aligned with (independent of) annual pycnocline variations in the ocean. These sloping black lines also allow us to estimate the westward phase speed of the SLH differences, plotted as a function of latitude in [Fig. 4](#) . They also allow us to assess qualitatively the phase relationships among the three variables, quantified utilizing coherence and phase statistics in [Fig. 5](#) .

In the Indian Ocean, the westward phase propagation of annual SLH differences at 10°, 14°, 18°, 22°, and 26°S can be seen extending across most of the ocean, restricted to the eastern and central ocean in the subtropics at 22° and 26°S ([Fig. 3a](#) ). These waves appear to originate near the west coasts of Australia and Indonesia, with amplification over the eastern and central Indian Ocean arising either from WSC forcing and/or from unstable interactions with the background shear flow ([Kang and Magaard 1980](#)). This is similar to the behavior of SLH anomalies for interannual coupled Rossby waves in the Indian Ocean observed by [White \(2000a\)](#). Over the eastern and central portions of the domain, westward phase propagation in annual SLH differences is matched by that in annual SST and MSW differences, as observed by [White \(2000a\)](#) on interannual period scales. The sloping black lines aligned with high SLH differences has covarying warm SST and poleward (negative) MSW differences displaced to the west by ~90° of phase. This phase relationship between warm SST and poleward MSW differences is the same at that observed in the Indian Ocean on interannual period scales ([White 2000a](#)), while the displacement of warm SST differences to the west of high SLH differences is different, with the two variables aligned on interannual period scales. This difference suggests that the coupling dynamics between ocean and atmosphere on annual and interannual period scales in the Indian Ocean are different.

The fixed alignment among the three variables in the Indian Ocean suggests that the annual cycle of SLH is coupled to that of MSW in the overlying atmosphere through its influence on the annual cycle of SST ([Fig. 3a](#) ). The westward displacement of warm SST differences from high SLH differences is consistent with oceanic thermal equilibrium between dissipation (e.g., SST-induced sensible-plus-latent heat loss to the atmosphere) and meridional geostrophic advection by the Rossby waves ([White et al. 1998](#)). The alignment of poleward MSW and warm SST differences is consistent with atmospheric potential vorticity equilibrium between planetary vorticity advection and stretching of the lower troposphere by SST-induced midtroposphere diabatic heating ([Palmer and Sun 1985](#)). Yet for both ocean and atmosphere, it remains to determine by observation and analysis whether these simplified thermodynamical and potential vorticity balances represent the true balances. Amplitudes of annual SLH differences are larger in the eastern and central Indian Ocean, consistent with the notion of a positive feedback between ocean and atmosphere there, and smaller in the western ocean where SLH, SST, and MSW differences lose alignment, from which we can infer that coupling is absent.

In the South Pacific Ocean, the westward phase propagation of annual SLH differences at 6°, 10°, 14°, and 18°S can be seen extending across the entire domain ([Fig. 3b](#) ). These SLH differences are not eastern intensified as in the Indian Ocean discussed above, nor were they on interannual period scales ([White 2000b](#)). Across the entire domain at all latitudes, SLH and SST differences are aligned. But SST and MSW differences are aligned across the entire domain only at 6° and 18°S; at 10° and 14°S they are aligned only in the eastern and central portions of the domain. In the eastern and central domain at each latitude, sloping black lines along high SLH differences overlie warm SST differences and poleward (negative) MSW differences. The phase relationship between SLH and SST differences is different than observed on interannual period scales ([White 2000b](#)), where warm SST anomalies were found displaced ~90° of phase to the west of high SLH anomalies. On the other hand, the phase relationship between SST and MSW differences is similar to those observed on interannual period scales ([White 2000b](#)). This difference indicates that coupling dynamics of annual and interannual waves in the South Pacific Ocean are different from one another, as in the Indian Ocean. The superposition of warm SST differences over high SLH differences is consistent with oceanic thermal equilibrium between dissipation (e.g., SST-induced sensible-plus-latent heat loss to the atmosphere) and deeper pycnocline displacements reducing the entrainment of colder subsurface water into the near-surface mixed layer ([White 2000a](#)). Poleward MSW differences overlie warm SST differences, the same phase relationship observed in the Indian Ocean. These phase relationships are maintained as latitude extends from the near-equatorial at 6°S to the high Tropics at 18°S. Amplitudes of annual SLH differences are larger in the central portion of the domain, suggesting that unstable wave growth due to coupling is confined to the eastern domain.

In the North Pacific Ocean, the westward phase propagation of annual SLH differences at 6°, 10°, 14°, and 18°N can be seen, but unlike in the Indian and South Pacific Oceans they do not extend uniformly across the domain, displaying a major disruption in the continuity of Rossby wave propagation in the central portion of the domain at 10°, 14°, and 18°N ([Fig. 3c](#) ). This latter disruption occurs near the longitude of the Hawaiian archipelago, indicated by the vertical dashed line. The waves east of the Hawaiian archipelago originate at or near the west coast of Central America and are much stronger than waves forming west of the Hawaiian archipelago. This eastern boundary source for annual Rossby waves is consistent with those observed in thermocline temperatures southeast of Hawaii ([White 1977](#)). On the other hand, westward phase propagation in annual SLH differences in the eastern tropical ocean is matched by that in annual SST and MSW differences, consistent with hypotheses that they are either in damped resonance with associated WSC differences (not shown) or they are coupled to the overlying atmosphere, as observed on interannual period scales ([White et al. 1998](#); [White 2000b](#)).

At each latitude in the North Pacific Ocean, the sloping black line along high SLH differences overlies warm SST differences, with poleward (positive) MSW differences displaced to the east by ~90° of phase ([Fig. 3c](#) ). The

superposition of warm SST differences and high SLH differences can be explained by the same thermodynamic balance observed in the South Pacific Ocean (Fig. 3b). The eastward displacement of poleward MSW differences from warm SST differences is consistent with low SLP differences occurring over warm SST differences. This latter phase relationship is different from that observed in the tropical Indian and South Pacific Oceans, perhaps due to the presence of the thermal equator near 10°N (Peixoto and Oort 1992), where warm SST differences can be expected to instigate cumulus convection, yielding low SLP differences directly overhead (Graham and Barnett 1987). Yet, this phase relationship differs from those observed on interannual period scales (White 2000b), indicating that the coupling dynamics of waves on annual and interannual period scales in the tropical North Pacific Ocean are different, as observed in the Indian and South Pacific Oceans. At 18°N, spatial modulation of SLH differences from the west coast of Central America to the Hawaiian archipelago indicates influence from a standing mode of WSC anomalies forcing the Rossby waves excited at the eastern boundary (White 1977). Even so, the earlier observation of annual Rossby waves southeast of the Hawaiian archipelago by White (1977) can now be seen (Fig. 3c) to be replaced by annual Rossby waves coupled to the overlying atmosphere.

5. Westward phase speeds of covarying SLH, SST, and MSW differences

Speeds of westward phase propagation of covarying SLH, SST, and MSW differences (solid circles in Fig. 4) are computed from tilts in sloping black lines in time–longitude diagrams of covarying SLH, SST, and MSW differences in Fig. 3, with error bars determined by possible changes in tilt that could occur to accommodate errors in interannual SLH anomalies. These error bars capture westward phase speeds indicated by solid circles in zonal wavenumber–frequency spectra (Fig. 2), consistent with those choices for wavenumber and frequency where westward-propagating waves share annual SLH, SST, and MSW spectral energy density. Superimposed upon these observed phase speeds is the meridional profile of westward phase speeds expected of free Rossby waves in the long-wave limit (Killworth et al. 1997).

The observed westward phase speeds in the Indian Ocean (Fig. 4, left) are larger (smaller) than those expected of free Rossby waves for latitude poleward (equatorward) of 14°S. The observed westward phase speeds in the Pacific Ocean (Fig. 4, middle and right) are larger (smaller) than those expected of free Rossby waves for latitude poleward (equatorward) of 10° latitude. Westward phase speeds in the Indian Ocean range from 0.17 to $0.11 \pm 0.03 \text{ m s}^{-1}$ from 10° to 26°S, respectively, while those in the tropical South Pacific Ocean range from 0.29 to $0.19 \pm 0.03 \text{ m s}^{-1}$ from 6° to 18°S, respectively. In the overlapping latitude band from 10° to 18°S, estimates in the Indian Ocean range from 0.17 to $0.13 \pm 0.03 \text{ m s}^{-1}$, while those in the South Pacific range from 0.26 to $0.19 \pm 0.03 \text{ m s}^{-1}$, larger by a factor of 1.5. The range of westward phase speeds in the Indian Ocean is also about half that in the South Pacific Ocean over the same latitude band. In the North Pacific Ocean, westward phase speeds range from 0.38 to $0.13 \pm 0.03 \text{ m s}^{-1}$ from 6° to 18°N, respectively (Fig. 4, right); this range is larger than in the Indian and South Pacific Oceans by more than a factor of 3, only slightly less than that given by the theory.

In each ocean, westward phase speeds decrease with increasing latitude, consistent with the theoretical meridional profile of westward phase speeds for free (uncoupled) Rossby waves. But these observed westward phase speeds show a much smaller decrease with latitude than expected of the free waves. This indicates that beta-refraction patterns expected of annual Rossby waves in the three oceans are less than those expected of free Rossby waves (White 1977). This is confirmed below in animation sequences of mapped annual SLH, SST, and MSW differences (Fig. 6).

6. Phase relationships between covarying SLH, SST, and MSW differences

Now, if we assume that covarying SLH, SST, and MSW differences arise from coupling between ocean and atmosphere (i.e., MSW differences are consistent with the dynamical equilibrium established in the lower troposphere in response to SST-induced air–sea sensible-plus-latent heat flux differences), then the thermodynamics linking the three variables are reflected in temporal and spatial phase relationships among them (White et al. 1998). Here we examine meridional profiles of spectral coherence and phase (Bendat and Piersol 1986, 361–424) computed between annual SLH and SST residuals (Fig. 5a) and annual SST and MSW residuals (Fig. 5b), computed in the same way as zonal wavenumber–frequency spectra in Fig. 2. These coherence and phase estimates were taken over zonal wavelengths ranging from 3000 to 5000 km in the Indian Ocean and from 4000 to 10000 km in the Pacific Ocean and annual periods indicated by solid circles in Fig. 2. In each ocean the dominant wavelength of the annual signal decreased with increasing latitude. We find the phase information displayed in Fig. 5 to be consistent with that determined by inspection of time–longitude diagrams in Fig. 3.

Meridional profiles of squared coherence and phase between annual SLH and SST residuals (Fig. 5a) in all three oceans finds it significant at the 90% confidence level at all latitudes (Jenkins and Watts 1968, 379–381), with phase differences distinct in each ocean; that is, $90^\circ \pm 30^\circ$ in the Indian Ocean, $0^\circ \pm 30^\circ$ in the South Pacific Ocean, and ranging from 0° to $90^\circ \pm 30^\circ$ in the North Pacific Ocean. The phase differences in the Indian Ocean find warm (cool) SST residuals displaced 90° of phase to the west of high (low) SLH residuals, while those in the South Pacific Ocean find warm (cool) SST residuals overlying high (low) SLH residuals. Phase differences in the North Pacific Ocean find warm (cool) SST residuals displaced to the west of (overlie) high (low) SLH residuals in the low (high) Tropics. In each case, these phase relationships are consistent with those observed in time–longitude diagrams in Fig. 3.

Phase differences between SLH and SST residuals of 90° are consistent with oceanic thermal equilibrium between dissipation (e.g., SST-induced sensible-plus-latent heat loss to the atmosphere) and meridional geostrophic advection by the Rossby waves ([White et al. 1998](#)). Phase differences of 0° are consistent with oceanic thermal equilibrium between dissipation (e.g., SST-induced sensible-plus-latent heat loss to the atmosphere) and pycnocline displacements reducing the entrainment of colder subsurface water into the near-surface mixed layer ([White 2000a](#)).

Meridional profiles of squared coherence and phase between annual SST and MSW residuals ([Fig. 5b](#)) in all three oceans finds squared coherence significant at the 90% confidence level at all latitudes ([Jenkins and Watts 1968](#), pp. 379–381), with phase differences in the Indian and South Pacific Oceans of $180^\circ \pm 30^\circ$ and in the North Pacific Ocean ranging from 45° to $90^\circ \pm 30^\circ$. The 180° phase difference in the Indian and South Pacific Oceans finds poleward (equatorward) MSW residuals overlying warm (cool) SST residuals, while the 90° phase difference in the North Pacific Ocean is consistent with low (high) SLP residuals overlying warm (cool) SST residuals. These phase relationships between annual residuals are consistent with those observed between annual differences in time–longitude diagrams in [Fig. 3](#).

Phase differences between SST and MSW residuals of 90° are consistent with the troposphere potential temperature balance wherein warm SST residuals, through their influence on air–sea sensible-plus-latent heat flux residuals, heat the overlying troposphere and instigate cumulus convection at midtroposphere levels, yielding low SLP residuals directly overhead ([Graham and Barnett 1987](#)). The alignment of poleward MSW and warm SST residuals is consistent with atmospheric potential vorticity balance between planetary vorticity advection and stretching of the lower troposphere by SST-induced midtroposphere diabatic heating ([Palmer and Sun 1985](#)). Whether these dynamical relationships are actually present remains for future examination.

These phase relationships between SLH, SST, and MSW residuals and differences in association with annual coupled Rossby waves have been observed before on interannual period scales. The 90° phase relationship between warm (cool) SST and high (low) SLH residuals was observed by [White et al. \(1998\)](#) and [White \(2000b\)](#) in the Pacific Ocean, while the 0° phase relationship was observed by [White \(2000a\)](#) in the Indian Ocean. The 0° phase relationship between poleward MSW and warm SST differences [i.e., 0° (180°) in the Northern (Southern) Hemisphere] was observed by [White et al. \(1998\)](#), [White \(2000b\)](#), and [White \(2000a\)](#) in the high tropical and extratropical Pacific and Indian Oceans. On the other hand, the 45° – 90° phase relationship, with poleward MSW residuals displaced to the east of warm SST residuals, was observed in the low tropical Pacific Ocean by [White \(2000b\)](#). This means that the phase relationships between SLH, SST, and MSW residuals associated with coupled Rossby waves observed in different geographical domains on different period scales in four separate studies are beginning to show consistency, with warm SST residuals displaced from 0° to 90° of phase to the west of high SLH residuals, and with poleward MSW residuals displaced from 0° to 90° of phase to the east of warm SST residuals.

7. Poleward refraction patterns of covarying SLH, SST, and MSW differences

Next we examine horizontal spatial patterns of covarying SLH, SST, and MSW differences in the Indian, North Pacific, and South Pacific Oceans. Free Rossby waves are characterized by a beta-refraction pattern with wave crests and troughs aligned so that the wave vector progressively points into the poleward direction with increasing zonal distance from the wave source ([White 1977](#)). This wave refraction stems from the decrease in westward phase speed with increasing latitude ([Veronis and Stommel 1956](#)). From the meridional profile of westward phase speeds of SLH differences ([Fig. 4](#)) we observed a similar decrease in westward phase speed with increasing latitude, but less than expected of free Rossby waves. Thus, we expect a refraction pattern similar to that of free Rossby waves but reduced in curvature. Moreover, because SLH differences covary with SST and MSW differences, we expect the refraction pattern to exist in all three variables as observed on interannual period scales by [White et al. \(1998\)](#) and [White \(2000a,b\)](#). We look for this in animation sequences of annual SLH, SST, and MSW differences extending over one year from January to January ([Fig. 6](#)).

These animation sequences display westward phase propagation in all three variables in each of the three ocean basins. In the Indian and South Pacific Oceans, the three variables appear to be coupled in the central and eastern portions of the two ocean basins, while in the North Pacific Ocean they appear to be coupled only over the eastern half of the basin westward to $\sim 160^\circ\text{W}$, with MSW differences in the western half of the basin more standing than propagating. In all three oceans the amplitude of SLH differences is more intense in the eastern half of the basins than in the western half, consistent with that observed in time–longitude diagrams ([Fig. 3](#)).

In all three basins, SLH, SST, and MSW differences are aligned with each other. In the North Pacific Ocean, they are aligned in the northeast–southwest direction, consistent with poleward refraction indicated by the decrease in westward phase speed with latitude ([Fig. 4](#)). In the Indian and South Pacific Oceans, they are aligned in the northwest–southeast direction, again consistent with poleward refraction indicated by the decrease in westward phase speed with latitude ([Fig. 4](#)). By examining the phase relationships relative to dashed reference lines ([Fig. 6](#)) we find warm SST differences displaced to the west of high SLH differences in the Indian and North Pacific Oceans, but approximately overlying high SLH differences in the South Pacific Ocean. Also we can see poleward (equatorward) MSW differences overlying warm (cool)

SST anomalies in the Indian and South Pacific Oceans, with poleward) MSW differences displaced to the east of warm (cool) SST differences in the North Pacific Ocean. These phase relationships are consistent with those determined by spectral coherence and phase in [Fig. 5](#).

These results reveal one salient aspect of covarying SLH, SST, and MSW differences in the three ocean basins; that is, they appear to have originated at the eastern boundary along the west coasts of Australia and North and South America, respectively. They do not appear to have been generated intrinsically in the interior of these ocean basins. The animation sequences in [Fig. 6](#) suggest that annual coupled Rossby waves in SLH differences are pumped at the west coasts of Australia and the Americas by the annual cycle of upwelling associated with MSW differences at these eastern boundaries, as proposed by [White and Saur \(1981\)](#) and modeled by [Mysak \(1983\)](#). In the Indian Ocean, this is consistent with interannual coupled Rossby waves generated at the west coast of Australia ([White 2000a](#)). Even so, this remains to be demonstrated in a coupled general circulation model.

8. Discussion and conclusions

In the present study we examine the annual cycle in SLH, SST, and MSW across the trade wind zone of the Indian and Pacific Oceans from 5° to 25° S for the period 1993–98. Zonal wavenumber–frequency spectra of monthly SLH, SST, and MSW residuals about the long-term annual mean for the 6 years yield peak spectral energy density for westward-traveling waves of annual period in all three variables for latitude bands 10° – 26° (6° – 18°) in the Indian (Pacific) Ocean. Moreover, annual variabilities among the three variables are phase locked to one another, with warm (cool) SST residuals overlying or displaced to the west of high (low) SLH residuals, and poleward (equatorward) MSW residuals overlying or displaced to the east of warm (cool) SST residuals. Animation sequences of the annual cycle for all three variables across the Indian and Pacific Oceans (with zonal mean removed) yields westward phase propagation for the covarying SLH, SST, and MSW differences, each sharing a poleward refraction pattern similar to but with less curvature than beta-refraction patterns associated with free baroclinic Rossby waves ([White 1977](#)); this is consistent with a smaller decrease in westward phase speed with increasing latitude. The westward phase propagation, poleward refraction, and phase relationship between ocean and atmosphere for annual coupled Rossby waves are similar to characteristics already observed for interannual coupled Rossby waves, for which different classes of theoretical waves have been derived ([White et al. 1998](#); [White 2000a,b](#)).

The specific phase relationships among the SLH, SST, and MSW residuals places constraints on the way in which the baroclinic structure of the upper ocean and the lower troposphere are coupled to one another. The fact that warm SST differences are displaced to the west or occur directly over high SLH differences suggests that SST-induced sensible-plus-latent heat flux differences balance some combination of meridional and vertical heat advection differences induced by the passage of the Rossby waves ([White et al. 1998](#)). The fact that poleward MSW differences are displaced to the east of (occur over) warm SST differences suggests that SST-induced sensible-plus-latent heat flux differences excite midtroposphere diabatic heating differences, which balance Newtonian cooling differences (which stretch the column and balance differences in the meridional advection of planetary vorticity) in the low- (high) latitude portion of trade wind zone ([Gill 1980](#); [Palmer and Sun 1985](#)). These potential temperature and potential vorticity balances in ocean and atmosphere remain to be confirmed by direct observation and analysis.

Yet, assuming these balances to hold, [White et al. \(1998\)](#) and [White \(2000a,b\)](#) have constructed theoretical ocean–atmosphere models for coupled Rossby waves, where SST-induced WSC anomalies produce a positive feedback to the baroclinic Rossby wave equation. Depending on whether meridional heat advection dominates vertical heat advection in the perturbation upper-ocean heat balance, and whether Newtonian cooling dominates potential vorticity considerations in the perturbation potential temperature and vorticity balance of the troposphere, at least four different classes of theoretical coupled Rossby waves have been developed ([White et al. 1998](#); [White 2000a,b](#)). The annual coupled Rossby waves in the present study yield relationships between SLH and SST differences, and between SST and MSW differences, which fall into one or the other of these four classes of theoretical coupled Rossby waves. There are two reasons for holding back on developing a general coupled Rossby wave model that would encompass the range of potentially important thermodynamical balances. One is the complexity of such a model, and the other is the necessity of confirming the proposed heat and vorticity balances in both the upper ocean and lower troposphere.

In the present study we have found coupled Rossby waves in the annual cycle of variability in the trade wind zone of the Indo-Pacific Ocean to be similar to those on interannual period scales. So, after examining coupled SLH, SST, and MSW variability on annual, biennial, and quadrennial period scales in the present study and in three earlier studies ([White et al. 1998](#); [White 2000a,b](#)) across both the tropical and subtropical Indo-Pacific Ocean, we find the zonal phase relationships among the three variables to be bounded by those given in the present study. So, if the proposed thermodynamical balances suggested by these phase relationships can be confirmed, then a general coupled Rossby wave model would be ready to be developed. Such a model would utilize the more complex mix of thermodynamical mechanisms responsible for the difference phase relationships between SLH and SST perturbations and between SST and MSW perturbations. We would expect a generalized coupled Rossby wave model to yield a dispersion relation for propagation and growth characteristics of theoretical coupled Rossby waves that would span the different classes of Rossby waves developed by [White et al. \(1998\)](#) and [White \(2000a,b\)](#).

If such a general model were available today, the question still remains why different phase relationships (and inferred thermodynamical balances) exist on different period scales and geographical domains. In the present study we found coupled Rossby wave activity on the annual cycle in the Indo-Pacific Ocean confined to the trade wind zone (Fig. 1), where high mean ZSW act as a catalyst for SST differences generating air–sea sensible-plus-latent heat flux differences. In response to this hypothetical forcing of the atmosphere by the ocean, we found poleward (equatorward) MSW differences overlying warm (cool) SST differences in all three oceans except near the intertropical convergence zone in the North Pacific Ocean, where it tended toward its equatorial phase relationship (Graham and Barnett 1987). What changes in background conditions are responsible for these geographical differences? Answering this question will require a thorough study of the atmospheric response to SST anomalies in the trade wind zone from 30°S to 30°N in both oceans. We also found warm (cool) SST differences overlying high (low) SLH differences in the South Pacific Ocean but displaced to the west of the latter in the Indian Ocean. What changes in background conditions are responsible for these geographical differences? Again, answering this question will require a thorough study of the upper-ocean diabatic heat budget in the trade wind zone from 30°S to 30°N in both oceans. Thus, for the thermodynamics of coupled Rossby waves to be understood will require a thorough examination of the heat and vorticity balances in both ocean and atmosphere, going beyond the exploratory stage of research conducted to date.

With the conclusion of the present study we can now compare annual Rossby wave activity in the eastern tropical North Pacific Ocean at 10°, 14°, and 18°N from 1993 to 1998 (Fig. 3c) with that observed from 10° to 19°N southeast of the Hawaiian archipelago from 1964 to 1965 by White (1977). Here we find SLH differences propagating westward from the west coast of Central America to the longitude of the Hawaiian archipelago, as in the earlier study with thermocline temperatures. But here we find SLH differences propagating in concert with SST and MSW differences, and presumably with WSC differences. This was not observed in the earlier work of White (1977). Moreover, these new observations are consistent with coupled Rossby wave activity observed over this same domain on interannual period scales (White et al. 1998; White 2000b). This suggests that covarying SLH and SST differences associated with the annual Rossby waves in the eastern tropical North Pacific Ocean southeast of Hawaii have a significant influence on the overlying troposphere. Coupling requires that SLP and MSW responses to SST differences be associated with WSC differences, providing a positive feedback from atmosphere to ocean that maintains the Rossby wave against dissipation. Thus, the present work indicates that the observed stability of annual Rossby waves, as they propagate from the eastern boundary to the longitude of the Hawaiian archipelago, is due to coupling with the overlying troposphere.

Acknowledgments

Warren White is supported by the National Aeronautics and Space Administration (NASA) as part of the TOPEX/Poseidon Extended Mission under contract JPL960886. He is also supported by NASA under contract NAG57653 in concert with the World Ocean Circulation Experiment (WOCE). Support also is given by the Scripps Institution of Oceanography of the University of California, San Diego. I thank Programmers Ted Walker and Jeffrey Annis for their efforts in conducting analyses utilized in this study, and I appreciate the efforts of Andrea Fincham in preparing the final figures and manuscript.

REFERENCES

- Bendat J. S., and A. G. Piersol, 1986: *Random Data: Analysis and Measurement Procedures*. John Wiley and Sons, 566 pp.
- Charnel R., D. Au, and G. Seckle, 1967: The trade wind zone oceanographic pilot study. Bureau of Commercial Fisheries Special Section Report Series, Nos. 552–557.
- Chelton D. B., and M. G. Schlax, 1996: Global observations of oceanic Rossby waves. *Science*, **272**, 234–238. [Find this article online](#)
- Cipollini P., D. Cromwell, M. S. Jones, G. D. Quartly, and P. G. Challenor, 1997: Concurrent altimeter and infrared observations of Rossby wave propagation near 34°N in the northeast Atlantic. *Geophys. Res. Lett.*, **24**, 889–892. [Find this article online](#)
- Cummins P. F., L. A. Mysak, and K. Hamilton, 1986: Wind stress curl generation of annual Rossby waves in the North Pacific. *J. Phys. Oceanogr.*, **16**, 1179–1189. [Find this article online](#)
- Dewar W. K., 1998: On “too fast” baroclinic planetary waves in the general circulation. *J. Phys. Oceanogr.*, **28**, 1739–1758. [Find this article online](#)
- Fu L.-L., E. J. Christensen, C. Y. Yamarone, M. Lefebvre, Y. Menard, M. Dorrer, and P. Escudier, 1994: TOPEX/Poseidon mission overview. *J. Geophys. Res.*, **99**, 24369–24381. [Find this article online](#)
- Gill A. E., 1980: Some simple solutions for heat induced tropical circulation. *Quart. J. Roy. Meteor. Soc.*, **106**, 447–462. [Find this article online](#)

- Graham N. E., and T. P. Barnett, 1987: Sea surface temperature, surface wind divergence, and convection over tropical oceans. *Science*, **238**, 657–659. [Find this article online](#)
- Graham N. E., and W. B. White, 1988: The El Niño cycle: A natural oscillator of the Pacific ocean–atmosphere system. *Science*, **240**, 1293–1302. [Find this article online](#)
- Halliwel G. R., P. Cornillion, and D. A. Byrne, 1991a: Westward-propagating SST anomaly features in the Sargasso Sea, 1982–88. *J. Phys. Oceanogr.*, **21**, 635–639. [Find this article online](#)
- Halliwel G. R., Y. J. Ro, and P. Cornillion, 1991b: Westward-propagating SST anomalies and baroclinic eddies in the Sargasso Sea. *J. Phys. Oceanogr.*, **21**, 1664–1680. [Find this article online](#)
- Hill K., I. Robinson, and P. Cipollini, 2000: Propagating characteristics of extratropical planetary waves observed in the ATSR global sea surface temperature record. *J. Geophys. Res.*, **105**, 21927–21945. [Find this article online](#)
- Jackson L. B., 1996: *Digital Filters and Signal Processing*. Kluwer Academic, 502 pp.
- Jenkins G. M., and D. G. Watts, 1968: *Spectral Analysis and Its Applications*. Holden-Day, 502 pp.
- Kalnay E., and Coauthors, 1996: The NCEP/NCAR 40-Year Reanalysis Project. *Bull. Amer. Meteor. Soc.*, **77**, 437–471. [Find this article online](#)
- Kang Y. Q., and L. Magaard, 1979: Stable and unstable Rossby waves in the North Pacific current as inferred from the mean stratification. *Dyn. Atmos. Oceans*, **3**, 1–14. [Find this article online](#)
- Kang Y. Q., and L. Magaard, 1980: Annual baroclinic Rossby waves in the central North Pacific. *J. Phys. Oceanogr.*, **10**, 1159–1167. [Find this article online](#)
- Kang Y. Q., J. M. Price, and L. Magaard, 1982: On stable and unstable Rossby waves in nonzonal oceanic shear flow. *J. Phys. Oceanogr.*, **12**, 528–537. [Find this article online](#)
- Kessler W. S., 1990: Observation of long Rossby waves in the northern tropical Pacific. *J. Geophys. Res.*, **95**, 5813–5219. [Find this article online](#)
- Killworth P. D., D. B. Chelton, and R. A. deZoeke, 1997: The speed of observed and theoretical long extratropical planetary waves. *J. Phys. Oceanogr.*, **27**, 1946–1966. [Find this article online](#)
- Magaard L., 1977: On the generation of baroclinic Rossby waves in the ocean by meteorological forces. *J. Phys. Oceanogr.*, **7**, 359–364. [Find this article online](#)
- Masumoto Y., and G. Meyers, 1998: Forced Rossby waves in the southern tropical Indian Ocean. *J. Geophys. Res.*, **103**, 27589–27602. [Find this article online](#)
- Meyers G., 1979: On the annual Rossby wave in the tropical North Pacific Ocean. *J. Phys. Oceanogr.*, **9**, 663–674. [Find this article online](#)
- Mysak L. A., 1983: Generation of annual Rossby waves in the North Pacific. *J. Phys. Oceanogr.*, **13**, 1910–1923. [Find this article online](#)
- Palmer T. N., and Z. Sun, 1985: A modeling and observational study of the relationship between sea surface temperature in the northwest Atlantic and the atmospheric general circulation. *Quart. J. Roy. Meteor. Soc.*, **111**, 947–975. [Find this article online](#)
- Pazan S., and W. B. White, 1987: Short-term climatic variability in the volume budget of the western tropical North Pacific Ocean during 1979–83. *J. Phys. Oceanogr.*, **17**, 440–454. [Find this article online](#)
- Peixoto J. P., and A. H. Oort, 1992: *Physics of Climate*. American Institute of Physics Press, 520 pp.
- Perigaud C., and P. Delecluse, 1993: Interannual sea level variations in the tropical Indian Ocean from GEOSAT and shallow-water simulations. *J. Phys. Oceanogr.*, **23**, 1916–1934. [Find this article online](#)
- Price J. M., and L. Magaard, 1983: Rossby wave analysis of subsurface temperature fluctuations along the Honolulu–San Francisco great circle. *J. Phys. Oceanogr.*, **13**, 258–268. [Find this article online](#)
- Qiu B., W. Miao, and P. Muller, 1997: Propagation and decay of forced and free baroclinic Rossby waves in off-equatorial oceans. *J. Phys. Oceanogr.*, **27**, 2405–2417. [Find this article online](#)
- Tai C.-K., W. B. White, and S. E. Pazan, 1989: GEOSAT crossover analysis in the tropical Pacific. Part 2. Verification analysis of altimetric sea level maps with XBT data and island sea level data. *J. Geophys. Res.*, **94**, 897–908. [Find this article online](#)

Veronis G., and H. Stommel, 1956: The action of the variable wind stress on a stratified ocean. *J. Mar. Res.*, **15**, 47–75. [Find this article online](#)

White W. B., 1977: Annual forcing of baroclinic long waves in the tropical North Pacific. *J. Phys. Oceanogr.*, **7**, 50–61. [Find this article online](#)

White W. B., 1983: Westward propagation of short-term climate variability in the western North Pacific Ocean from 1964–1974. *J. Mar. Res.*, **41**, 113–125. [Find this article online](#)

White W. B., 1985: The resonant response of interannual baroclinic Rossby waves to wind forcing in the eastern midlatitude North Pacific. *J. Phys. Oceanogr.*, **15**, 403–415. [Find this article online](#)

White W. B., 2000a: Coupled Rossby waves in the Indian Ocean on interannual timescales. *J. Phys. Oceanogr.*, **30**, 2972–2988. [Find this article online](#)

White W. B., 2000b: Tropical coupled Rossby waves in the Pacific ocean–atmosphere system. *J. Phys. Oceanogr.*, **30**, 1245–1264. [Find this article online](#)

White W. B., and J. F. T. Saur, 1981: A source of annual baroclinic waves in the eastern subtropical North Pacific. *J. Phys. Oceanogr.*, **11**, 1452–1462. [Find this article online](#)

White W. B., and J. F. T. Saur, 1983: Sources of interannual baroclinic waves in the eastern subtropical North Pacific. *J. Phys. Oceanogr.*, **13**, 1035–1046. [Find this article online](#)

White W. B., and C.-K. Tai, 1992: Reflection of interannual Rossby waves at the maritime western boundary of the tropical Pacific. *J. Geophys. Res.*, **97**, 14305–14322. [Find this article online](#)

White W. B., and C.-K. Tai, 1995: Inferring interannual changes in global heat storage from TOPEX altimetry. *J. Geophys. Res.*, **100**, 24943–24954. [Find this article online](#)

White W. B., G. Meyers, J. Donguy, and S. Pazan, 1985a: Short-term climatic variability of the Pacific Ocean during 1979–1982. *J. Phys. Oceanogr.*, **15**, 917–935. [Find this article online](#)

White W. B., S. Pazan, and B. Li, 1985b: Processes of short-term climate variability in the baroclinic structure of the western North Pacific. *J. Phys. Oceanogr.*, **15**, 386–402. [Find this article online](#)

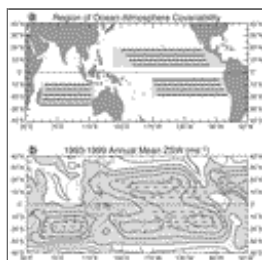
White W. B., Y.-H. He, and S. E. Pazan, 1989: Off-equatorial westward propagating Rossby waves in the tropical Pacific during the 1982–83 and 1986–87 ENSO events. *J. Phys. Oceanogr.*, **19**, 1397–1406. [Find this article online](#)

White W. B., N. Graham, and C.-K. Tai, 1990a: Reflection of annual Rossby waves at the maritime western boundary of the tropical Pacific. *J. Geophys. Res.*, **95**, 3101–3116. [Find this article online](#)

White W. B., C.-K. Tai, and J. DiMento, 1990b: Annual Rossby wave characteristics in the California Current region from the GEOSAT exact repeat mission. *J. Phys. Oceanogr.*, **20**, 1297–1311. [Find this article online](#)

White W. B., Y. Chao, and C.-K. Tai, 1998: Coupling of biennial oceanic Rossby waves with the overlying atmosphere in the Pacific basin. *J. Phys. Oceanogr.*, **28**, 1236–1251. [Find this article online](#)

Figures



[Click on thumbnail for full-sized image.](#)

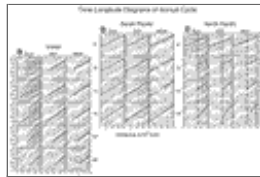
FIG. 1. (a) Map of the Indo–Pacific Ocean showing the shaded region where monthly residuals of TOPEX/Poseidon sea level height (SLH) and NCEP–NCAR sea surface temperature (SST) and meridional surface wind (MSW) about the annual mean are found to covary with one another. Zonal dark lines are placed at 4° latitude increments ranging from 6° to 26° latitude and delineate longitudes along which SLH, SST, and MSW differences are analyzed, with the degree of alignment and phase

relationships between variables established using wavelet coherence and phase analysis. (b) The distribution of the annual mean zonal surface wind (ZSW) from 1993 to 1998, with easterly trade winds (westerly winds) shaded (unshaded). Zonal dark lines from (a) are reproduced on (b), showing where covariability among SLH, SST, and MSW residuals occurs in relation to the annual mean ZSW distribution



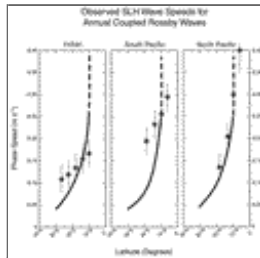
Click on thumbnail for full-sized image.

FIG. 2. Propagation zonal wavenumber–frequency spectra (Bendat and Piersol 1986, pp. 361–424) of monthly SLH, SST, and MSW residuals about the annual mean are computed from time–longitude diagrams along zonal dark lines in Fig. 1. These residuals have been pass filtered from 6 to 18 months and extend over 60 months from Jul 1993 to Jun 1998 and in longitude over 6600 km in the Indian Ocean, 9500 km in the South Pacific Ocean, and 11 000 km in the North Pacific Ocean. Spectra for (a) the Indian Ocean, (b) the South Pacific Ocean, and (c) the North Pacific Ocean are displayed. Spectral energy densities are contoured at $10^2 \text{ m}^2/(\text{s}^{-1} \text{ m}^{-1})$ for SLH, $10^4 \text{ }^\circ\text{C}^2/(\text{s}^{-1} \text{ m}^{-1})$ for SST, and $10^5 (\text{m s}^{-1})^2/(\text{s}^{-1} \text{ m}^{-1})$ for MSW. Contours are significantly different from adjacent contours at the 90% confidence level (Jenkins and Watts 1968, 77–89). Hatched regions are for effect. Solid circles are superimposed on each spectrum by the author to show wavenumber–frequency regions of shared peak spectral energy density. The sloping solid line delineates the free Rossby wave dispersion curve (see text for details)



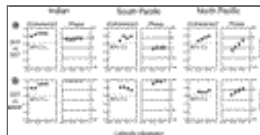
Click on thumbnail for full-sized image.

FIG. 3. Representative time–longitude diagrams for long-term monthly mean SLH, SST, and MSW differences about the long-term annual mean for latitudes ranging from 6° to 26°S in the Indian and Pacific Oceans over longitudes given by corresponding solid lines in Fig. 1, extending in time over 60 months from Jul 1993 to Jun 1998. Diagrams are displayed for (a) the Indian Ocean, (b) the South Pacific Ocean, and (c) the North Pacific Ocean. Negative (positive) differences are shaded (unshaded) with contours of 0.005 m for SLH differences, 0.05°C for SST differences, and 0.1 m s^{-1} for MSW differences. The sloping black line in each time–longitude diagram is for reference, allowing the reader to assess the degree of alignment and phase relationships among the three variables at each latitude. The slope of this line is used to estimate the westward phase speed of covarying SLH, SST, and MSW differences at each latitude



Click on thumbnail for full-sized image.

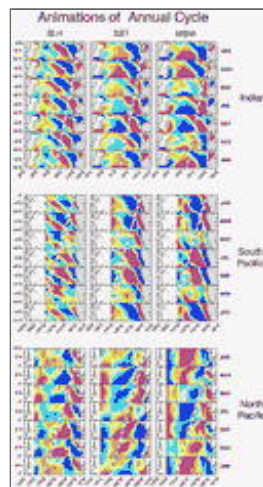
FIG. 4. Meridional profiles of westward phase speeds for SLH differences (closed circles) referenced to theoretical speeds for free Rossby waves (solid line), computed by Killworth et al. (1997). These observed westward phase speeds were computed from the tilt in the sloping black lines displayed in time–longitude diagrams in Fig. 3. Error bars represent the estimated variation in tilt in Fig. 3 taking into account errors in annual SLH differences. Error bars encompass phase speeds determined from the solid circles in propagation spectra in Fig. 2



Click on thumbnail for full-sized image.

FIG. 5. Meridional profiles of squared coherence and zonal phase lag between (a) SLH and SST residuals and (b) SST and MSW residuals, computed from time–longitude diagrams of monthly SLH, SST, and MSW residuals about the annual mean along zonal dark lines in Fig. 1. These residuals have been pass filtered from 6 to 18 months, extending in time over 60 months from Jul 1993 to Jun 1998 and in longitude over 6600 km in the Indian Ocean, 9500 km in the South Pacific Ocean, and 11 000 km in the

North Pacific Ocean. Estimates were extracted from propagation zonal wavenumber–frequency coherence and phase diagrams at the location of solid circles in [Fig. 2](#). Squared coherence estimates (solid circles) are statistically significant at the 90% confidence level, the latter given by the horizontal dashed line. Maximum error estimates of $\pm 30^\circ$ in phase difference depends both on 8 degrees of freedom in spectral coherence and its 90% confidence level ([Jenkins and Watts 1968](#), 379–381)



[Click on thumbnail for full-sized image.](#)

FIG. 6. Animation sequences of maps for long-term monthly mean SLH, SST, and MSW differences about the long-term annual mean, with zonal mean and trend removed. Positive (negative) SLH differences range from yellow to red (light blue to dark blue), with contour intervals of 0.005 m for SLH anomalies, 0.05°C for SST anomalies, and 0.05 m s^{-1} for MSW anomalies. Sloping dashed lines are provided for reference, allowing the reader to assess the degree of alignment and phase relationships between wave crests and troughs among the three variables. The sense of propagation comes from following annual differences of similar sign from one map to the next in each animation sequence

Corresponding author address: Dr. Warren B. White, Scripps Institution of Oceanography, University of California, San Diego, La Jolla, CA 92093-0230. E-mail: wwhite@ucsd.edu

[top](#) ▲



© 2008 American Meteorological Society [Privacy Policy and Disclaimer](#)

Headquarters: 45 Beacon Street Boston, MA 02108-3693

DC Office: 1120 G Street, NW, Suite 800 Washington DC, 20005-3826

amsinfo@ametsoc.org Phone: 617-227-2425 Fax: 617-742-8718

[Allen Press, Inc.](#) assists in the online publication of AMS journals.